AIAA 81-1004R

Conservative Full Potential, Implicit Marching Scheme for Supersonic Flows

Vijaya Shankar*
Rockwell International Science Center, Thousand Oaks, California

An aerodynamic prediction technique based on the full potential equation in conservation form is developed for the treatment of supersonic flows. This technique bridges the gap between simplistic linear theory methods and complex Euler solvers. A local density linearization concept and a second-order-accurate retarded density scheme, both producing the correct artificial viscosity, are introduced in developing an implicit marching scheme for solving the scalar potential ϕ. Results for conical flows over delta wings, cones, and wing-body combinations, and for nonconical flows over bodies of revolution at angles of attack are compared with Euler and nonconservative full potential calculations and experimental data. The present formulation requires an order of magnitude less computer time and significantly less computer memory over Euler methods.

I. Introduction

AERODYNAMIC prediction techniques that can handle significant geometric complexity for use in supersonic or hypersonic configuration design are based on either hypersonic impact methods[1] or linear theory analysis,[2] both of which require minimum response time and cost. However, shortcomings are present in both the impact and linearized methods. Aside from these simplified techniques, limited capabilities also exist for calculating supersonic flowfields using very complex Euler codes,[3-6] using either shock capturing[3] or shock fitting[4-6] methods. The use of these codes as viable aerodynamic prediction techniques for configuration design is, however, not practical due to their slow response time (requirement of large computer memory) and excessive computer cost per run due to strict stability requirements. Thus, we have on one end of the spectrum, very simplified codes that require minimum computer time to provide less accurate results and, on the other end, very complex Euler codes that require excessive computer time to provide quality results.

In an attempt to bridge this gap between simplistic linear theory methods and complex Euler solvers, several methodologies such as the second-order potential analysis,[7] hypersonic small disturbance theory,[8] and, more recently, nonconservative full potential methods[9,10] have been considered by various investigators. The second-order theory,[7] in spite of the significant improvements reported, suffers from the lack of nonlinearity in resolving proper cross flow shocks and sonic lines. Also, the singularities inherent in the formulation create difficulties in the numerical treatment of subsonic leading edges. The finite difference analysis of the hypersonic small disturbance theory[8] indicates that the solution procedure is as complex as that for the Euler equation and not particularly responsive to preliminary design level of effort.

Recently, Grossman[9] and Grossman and Siclari[10] have computed supersonic flowfields over conical and nonconical cambered and twisted delta wings with remarkable success using the nonconservative full potential equation and a transonic relaxation method. However, their approach is made complicated by the use of global conformal mappings which apply only to certain classes of configurations. Also, the nonconservative form of the full potential equation is in terms of second derivatives of the potential ϕ, which, when a transformation is applied, generates a large number of first and second derivative transformation terms.

The full potential method proposed in this paper is significantly different from that of Refs. 9 and 10. First of all, the method is based on the conservative form of the full potential equation, since for a shock capturing procedure to conserve mass across the shock wave,[11] it is essential that the equation be cast in conservation form.[12] Second, the method can accommodate a numerical or analytical mapping procedure that is either orthogonal or nonorthogonal without complicating the form of the equation, in contrast to Refs. 9 and 10. Third, the method is based on an approximate factorization implicit algorithm that can yield convergence much faster than the conventional successive line over-relaxation method.[10] Finally, the method is not an adaptation of a transonic code using type dependent operators, but a scheme specifically developed and tailored for supersonic marching problems using a density linearization concept and has no step size restrictions.

To validate the present methodology, results are shown for a variety of conical and nonconical geometries and are compared with Euler solutions and full potential results of Refs. 9 and 10. Results indicate that the method works just as fast and efficient for nonconical flows as in the case of conical geometry treatment. Results also indicate that the method is very useful in computing very high-speed flows ($M_\infty \sim 2$-6) for the moderate flow deflection angles ($\alpha \sim 4$-10 deg) where the neglect of entropy generation does not seriously distort the main features of the flowfield.

The present method can also handle more complicated geometries (realistic wing-body combinations) than the ones reported in the paper, but requires a suitable grid generation routine, especially near wing-body junction regions. In a subsequent paper,[13] results for nonconical wing-body flows will be presented along with a formal method of characteristics treatment for cross flow signal propagation.

II. Formulation

The conservative form of the full potential equation in Cartesian coordinates x, y, z can be written as

$$\frac{\partial(\rho u)}{\partial x} + \frac{\partial(\rho v)}{\partial y} + \frac{\partial(\rho w)}{\partial z} = 0 \tag{1}$$

where ρ is the density and u, v, w are the velocity components. They are calculated as the gradient of the potential ϕ,

$$u = \phi_x; \quad v = \phi_y; \quad w = \phi_z \tag{2}$$

Presented as Paper 81-1004 at the AIAA Fifth Computational Fluid Dynamics Conference, Palo Alto, Calif., June 22-23, 1981; submitted June 24, 1981; revision received March 22, 1982.

*CFD Project Leader. Associate Fellow AIAA.

The density ρ is computed from the isentropic formula

$$\rho=\left[1-\frac{\gamma-1}{2}M_\infty^2(u^2+v^2+w^2-1)\right]^{1/\gamma-1} \tag{3}$$

If the density is normalized with respect to the freestream value, then the speed of sound a is given by

$$a^2=\rho^{\gamma-1}/M_\infty^2 \tag{4}$$

where M_∞ is the freestream Mach number.

The objective of the paper is to solve for the scalar potential ϕ from Eq. (1) subject to the surface tangency condition $\phi_n=0$ (n is normal to the body surface). Examining Eq. (1), it is very clear that ϕ appears in a nonlinear form due to the presence of the density term inside the derivative. The approach to be described here is a method that treats the density term in such a way that it produces the correct artificial viscosity needed for shock capturing and that enables one to solve for ϕ with relative ease.

In order to apply the surface tangency condition at the actual body location, a body-fitted coordinate transformation is essential. Introducing a body-fitted coordinate transformation, $\zeta=\zeta(x,y,z)$, $\eta=\eta(x,y,z)$, and $\xi=\xi(x,y,z)$, Eq. (1) transforms to

$$\left(\rho\frac{U}{J}\right)_\zeta+\left(\rho\frac{V}{J}\right)_\eta+\left(\rho\frac{W}{J}\right)_\xi=0 \tag{5}$$

where U, V, and W are the contravariant velocity components. Introducing the following notation for convenience:

$$U=U_1,\quad V=U_2,\quad W=U_3$$

$$x=x_1,\quad y=x_2,\quad z=x_3$$

$$\zeta=X_1,\quad \eta=X_2,\quad \xi=X_3$$

the contravariant velocities and density are given by

$$U_i=\sum_{j=1}^{3}a_{ij}\phi_{x_j}\qquad i=1,2,3$$

$$a_{ij}=\sum_{k=1}^{3}\frac{\partial X_i}{\partial x_k}\frac{\partial X_j}{\partial x_k}\qquad i=1,2,3,\quad j=1,2,3$$

$$\rho=\left[1-\left(\frac{\gamma-1}{2}\right)M_\infty^2\{U\phi_\zeta+V\phi_\eta+W\phi_\xi-1\}\right]^{1/(\gamma-1)} \tag{6}$$

The Jacobian of the transformation J is represented by

$$J=\frac{\partial(\zeta,\eta,\xi)}{\partial(x,y,z)}=\begin{bmatrix}\zeta_x & \zeta_y & \zeta_z\\ \eta_x & \eta_y & \eta_z\\ \xi_x & \xi_y & \xi_z\end{bmatrix} \tag{7}$$

Equation (5) is in terms of a general coordinate system (ζ,η,ξ) and can accommodate any kind of mapping procedure, either analytical (conformal mapping) or numerical type. Any numerical marching procedure applied to Eq. (5) to simulate a supersonic flow should have a truncation error whose leading terms represent a correct artificial viscosity. This is essential to ensure marching numerical stability and to exclude the formation of expansion shocks which are unphysical and correspond to a decrease in entropy. The nature of the required artificial viscosity can be studied by an analysis[14] of the canonical form of Eq. (5), which indicates that for stability, the form of artificial viscosity be

$$\frac{\rho}{Ja^2}\left\{1-\frac{a^2}{q^2}\right\}[\Delta\zeta U\{U\phi_{\zeta\zeta\zeta}+V\phi_{\eta\zeta\zeta}+W\phi_{\xi\zeta\zeta}\}$$
$$+\Delta\eta V\{U\phi_{\zeta\eta\eta}+V\phi_{\eta\eta\eta}+W\phi_{\xi\eta\eta}\}$$
$$+\Delta\xi W\{U\phi_{\zeta\xi\xi}+V\phi_{\eta\xi\xi}+W\phi_{\xi\xi\xi}\}] \tag{8}$$

assuming that U, V, W are positive. What this implies is that if the flowfield is hyperbolic ($q>a$), then solution can be obtained by marching along the hyperbolic flow direction s. Once the total velocity q becomes less than a, then marching along s is not possible. This is reflected in the fact that the effective artificial viscosity given by Eq. (8) is now negative.

Now we will proceed with the numerical procedure for solving Eq. (5), and show the resemblance of the resulting artificial viscosity to that of Eq. (8).

A. Treatment of $\frac{\partial(\rho U/J)}{\partial\zeta}$ in Eq. (5)

Consider the direction ζ to be the marching direction. The condition to be satisfied for this to be true will become evident at the end of this analysis. Both the density ρ and the contravariant velocity U are functions of the potential ϕ and the transformation metrics, as represented in Eq. (6). In order to finite difference this ζ derivative quantity in terms of ϕ only will require some linearization treatment of the density. This will be termed the "local density linearization" procedure. In the transonic formulation described by Holst,[15] the density is upwind biased and computed at the old level, while retaining central differencing for the (U/J) term at the current level. Such an upwind density bias is shown to produce the right artificial viscosity in Ref. 14. Referring to Fig. 1, for a pure supersonic marching problem (say we want to march from the ith plane to the $i+1$th plane), a transonic relaxation procedure[15] in the marching direction ζ is not appropriate because the solution ϕ at the $i+1$th plane is not influenced by the $i+2$th plane. Hence, the following marching procedure is developed.

Given the ϕ information at all the previous planes i, $i-1$, $i-2,\ldots$, the problem is to compute ϕ at the $i+1$th plane. Now, expand the unknown $\rho=\rho(\phi)$ in terms of a neighboring known state denoted here by a subscript 0 (ith plane information would represent the neighboring known state for the $i+1$th plane).

$$\rho=\rho_0+\left(\frac{\partial\rho}{\partial\phi}\right)_0\Delta\phi+\ldots \tag{9}$$

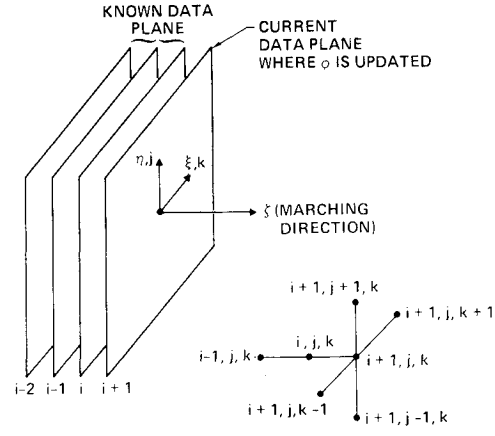

Fig. 1 Implicit computational molecule.

where $\Delta\phi=\phi-\phi_0$ and $\partial\rho/\partial\phi$ can be shown to be a differential operator[16]

$$\left(\frac{\partial\rho}{\partial\phi}\right)_0 \Delta\phi=-\frac{\rho_0}{a_0^2}\left\{U_0\frac{\partial}{\partial\zeta}+V_0\frac{\partial}{\partial\eta}+W_0\frac{\partial}{\partial\xi}\right\}(\phi-\phi_0) \quad (10)$$

Substituting Eqs. (9) and (10) into the first term in Eq. (5), we get

$$\frac{\partial(\rho U/J)}{\partial\zeta}\doteq\frac{\partial}{\partial\zeta}\left(\left[\rho_0-\frac{\rho_0}{a_0^2}\left\{U_0\frac{\partial}{\partial\zeta}+V_0\frac{\partial}{\partial\eta}+W_0\frac{\partial}{\partial\xi}\right\}(\phi-\phi_0)\right]\frac{U}{J}\right) \quad (11)$$

Substituting for U in terms of ϕ from Eq. 6 and rearranging Eq. (11) in terms of the potential difference $\Delta\phi$, we get

$$\frac{\partial(\rho U/J)}{\partial\zeta}\doteq\frac{\partial}{\partial\zeta}\left\{\frac{\rho_0}{J}\left[\left(a_{11}-\frac{U^2}{a^2}\right)_0\frac{\partial}{\partial\zeta}\Delta\phi+\left(a_{12}-\frac{UV}{a^2}\right)_0\times\frac{\partial}{\partial\eta}\Delta\phi+\left(a_{13}-\frac{UW}{a^2}\right)_0\frac{\partial}{\partial\xi}\Delta\phi+U_0\right]\right\} \quad (12)$$

where the speed of sound a_0, the density ρ_0, and the contravariant velocities U_0, V_0, W_0, represent information at the neighboring known plane. The ζ derivative term of Eq. (12) will now be one-sided differenced. Assuming U is positive,

$$\frac{\partial(\ )}{\partial\zeta}=\frac{1}{\Delta\zeta}\{(\ )_{i+1,j,k}-(\ )_{i,j,k}\} \quad (13)$$

An upwind differencing of the form Eq. (13) applied to Eq. (12) can be shown to produce a truncation term whose leading term is

$$\frac{\rho}{Ja^2}\left\{1-\frac{a^2a_{11}}{U^2}\right\}U^2\phi_{\zeta\zeta\zeta}\Delta\zeta \quad (14)$$

which will always represent a positive artificial viscosity as long as

$$\frac{U^2}{a_{11}}>a^2 \quad (15)$$

The preceding relation sets the condition for ζ to be the marching direction, for if U^2/a_{11} is less than the square of the local speed of sound, then the artificial viscosity becomes negative and a marching instability will occur. This also implies that the projection of the total velocity vector q in the direction normal to the $\zeta=$const plane (η,ξ plane) is supersonic. For example, in a spherical system, for the radial direction r to be the marching direction, the radial velocity q_r must be supersonic. The similarity between the artificial viscosity term given by Eq. (14) and the first term appearing in Eq. (8) can be noted. When backward differenced, the terms in Eq. (12) will lead to a diagonally dominant tridiagonal set of equations for the unknown $\Delta\phi$ when coupled with the other two terms in Eq. (5). The mixed derivative terms like $\phi_{\zeta\eta}$ and $\phi_{\zeta\xi}$ appearing in Eq. (12) will be upwind biased, depending on the sign of the coefficient multiplying them to preserve diagonal dominance and to provide the right artificial viscosity.

B. Treatment of $\frac{\partial(\rho V/J)}{\partial\eta}$ in Eq. (5)

This term will be written at the $i+1$th plane to make the resulting scheme fully implicit.

$$\frac{\partial(\rho V/J)}{\partial\eta}=\frac{\partial}{\partial\eta}\left\{\frac{\rho}{J}(a_{21}\phi_\zeta+a_{22}\phi_\eta+a_{23}\phi_\xi)\right\} \quad (16)$$

The density term ρ in Eq. (16) cannot be represented at the $i+1$th plane since that would result in a very complicated nonlinear form for ϕ. Hence, a density approximation is introduced by setting $\rho=\rho^*$ where $\rho^*=\rho_0$ for conical flow treatment. In the case of nonconical flows, while advancing from i to the $i+1$th plane, several iterations are performed within each cross flow plane (η,ξ) to refine the density ρ^* to properly account for the axial geometry variation. This is done by initially setting ρ^* to ρ_0 and then subsequently refining it by setting ρ^* to the previous iterate value of ρ at the current plane. In many cases where the axial variation of the geometry is gradual (especially for smaller step size calculations) it was found that setting $\rho^*=\rho_0$ even for nonconical flows produced very good results without having to refine the density subsequently.

Writing Eq. (16) in terms of the potential difference $\Delta\phi$

$$\frac{\partial(\rho V/J)}{\partial\eta}\doteq\left(\frac{\rho^*a_{21}}{J}\frac{\Delta\phi}{\Delta\zeta}\right)_\eta+\left(\frac{\rho^*a_{22}}{J}\frac{\partial}{\partial\eta}\Delta\phi\right)_\eta+\left(\frac{\rho^*a_{23}}{J}\frac{\partial}{\partial\xi}\Delta\phi\right)_\eta+\left(\frac{\rho^*a_{22}}{J}\frac{\partial}{\partial\eta}\phi_0\right)_\eta+\left(\frac{\rho^*a_{23}}{J}\frac{\partial}{\partial\xi}\phi_0\right)_\eta \quad (17)$$

A simple central differencing for the various terms in Eq. (17) will not be sufficient as that would not provide the desired artificial viscosity given by Eq. (8), required for shock capturing. To simulate an artificial viscosity of the form given by Eq. (8), the density will be upwind biased based on the previous work reported in Refs. 14-16. The density ρ^* will be replaced by a modified density $\tilde\rho^*$ given by

$$(\tilde\rho^*)_{j+\frac12,k}=(1-\nu_{j+\frac12,k})(\rho^*)_{j+\frac12,k}+\tfrac12\nu_{j+\frac12,k}\{(1+\theta)(\rho^*)_{j+2m,k}+(1-\theta)(\rho^*)_{j-1+2m,k}\} \quad (18)$$

where $m=0$ when $(V_0)_{j+\frac12,k}>0$ and $m=+1$ when $(V_0)_{j+\frac12,k}<0$. When θ is set to zero, first-order accurate density biasing is achieved while $\theta=2$ gives second-order accuracy. The artificial viscosity coefficient $\nu_{j+\frac12,k}$ is computed as follows:

$$\nu_{j+\frac12,k}=[1-(a_0^2/q_0^2)]_{j+s,k} \quad (19)$$

where $s=0$ for $V_{j+\frac12,k}>0$ and $s=1$ for $V_{j+\frac12,k}<0$.

Treatment of density as represented by Eqs. (18) and (19) would always produce a positive artificial viscosity as long as the local total velocity q_0 is supersonic. If that becomes subsonic, then the marching procedure would fail and the problem have to be treated as a transonic problem.

The treatment of the $(\partial/\partial\xi)[\rho W/J]$ term in Eq. (5) is very similar to the just described $(\partial/\partial\eta)[\rho V/J]$ term, except that the density biasing will be in the ξ direction and will be based on the sign of W.

C. Implicit Factorization Algorithm

Combining the various terms in Eqs. (12) and (17), and the terms arising from $(\partial/\partial\xi)[\rho W/J]$ will result in a fully implicit representation of Eq. (5) which cannot be solved without introducing an approximate factorization procedure. After some rearrangement of the terms, the factored implicit scheme becomes

$$\left[1+\frac{A_3}{\beta\Delta\zeta}\frac{\partial}{\partial\xi}+\frac{1}{\beta}\frac{\partial}{\partial\xi}\left(\frac{\tilde\rho^*}{J}\frac{a_{31}}{\Delta\zeta}\right)+\frac{1}{\beta}\frac{\partial}{\partial\xi}\frac{\tilde\rho^*a_{33}}{J}\frac{\partial}{\partial\xi}\right]\times\left[1+\frac{A_2}{\beta\Delta\zeta}\frac{\partial}{\partial\eta}+\frac{1}{\beta}\frac{\partial}{\partial\eta}\left(\frac{\tilde\rho^*a_{21}}{J\Delta\zeta}\right)+\frac{1}{\beta}\frac{\partial}{\partial\eta}\frac{\tilde\rho^*a_{22}}{J}\frac{\partial}{\partial\eta}\right]\Delta\phi=R \quad (20)$$

This equation has the form

$$L_\xi L_\eta(\Delta\phi) = R \tag{21}$$

and it is implemented as follows:

$$L_\xi(\Delta\phi)^* = R \qquad L_\eta(\Delta\phi) = (\Delta\phi)^* \qquad \phi = \phi_0 + \Delta\phi \tag{22}$$

The various quantities appearing in Eq. (20) are given by

$$\beta = \frac{A_1}{(\Delta\zeta)^2} \qquad A_1 = \frac{\rho_0}{J}\left(a_{11} - \frac{U^2}{a^2}\right)_0$$

$$A_2 = \frac{\rho_0}{J}\left(a_{12} - \frac{UV}{a^2}\right)_0 \qquad A_3 = \frac{\rho_0}{J}\left(a_{13} - \frac{UW}{a^2}\right)_0 \tag{23}$$

and the right-hand side term R consists of various known quantities.

The algorithm Eq. (22) requires only scalar tridiagonal inversions. Also, the scheme does not pose any restrictions on the direction of sweep that are present in the successive line over-relaxation method.[9,10]

D. Freestream Truncation Errors

To subtract out any numerical truncation error due to incomplete metric cancellation,[16] it is essential to add the terms (especially for a highly stretched nonorthogonal grid)

$$\frac{\partial}{\partial\zeta}\left(\frac{\rho_\infty U_\infty}{J}\right) + \frac{\partial}{\partial\eta}\left(\frac{\rho_\infty V_\infty}{J}\right) + \frac{\partial}{\partial\xi}\left(\frac{\rho_\infty W_\infty}{J}\right) \tag{24}$$

to the right-hand side of Eq. (20).

E. Boundary Conditions

In order to solve for $\Delta\phi$ from Eq. (20), boundary conditions will have to be prescribed at all four boundaries as shown in Fig. 2 at the current $i+1$th plane. While performing the L_ξ operator in Eq. (21), boundary conditions in terms of $\Delta\phi^*$ will be required along the $k=2$ and $k=K\text{MAX}-1$ boundaries. For a pure angle-of-attack problem, $k=2$ and $k=K\text{MAX}-1$ can be considered as planes of symmetry across which all flow variables reflect. The quantity $\Delta\phi^*$, even though it has no physical significance, can be safely set

$$(\Delta\phi)^*_{i+1,j,K\text{MAX}} = (\Delta\phi)^*_{i+1,j,K\text{MAX}-2}$$

$$(\Delta\phi)^*_{i+1,j,1} = (\Delta\phi)^*_{i+1,j,3} \tag{25}$$

The L_η operator would require boundary conditions along $j=2$ and $j=J\text{MAX}$ in terms of $\Delta\phi$. Since $j=2$ is the body, the surface tangency condition

$$V = a_{21}\phi_\xi + a_{22}\phi_\eta + a_{23}\phi_\xi = 0 \tag{26}$$

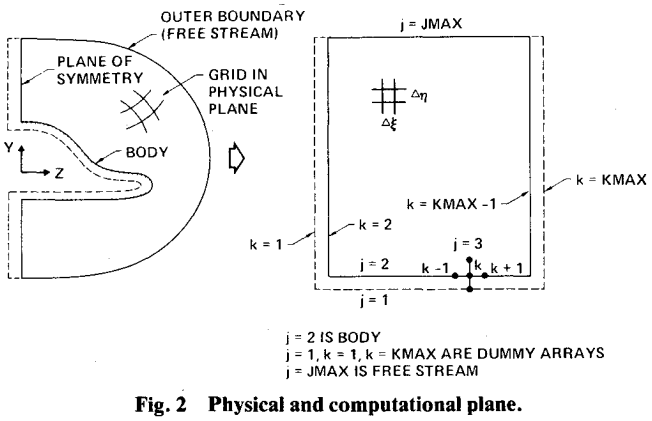

Fig. 2 Physical and computational plane.

will be set at all points $(i+1,2,k)$. Along $j=J\text{MAX}$, freestream $\Delta\phi$ will be imposed.

F. Grid System

As shown in Fig. 2, the physical space (x,y,z) is transformed into a body-fitted (ζ,η,ξ) computational space. The transformation is performed numerically by using the elliptic grid generation techniques originally developed by Thompson et al.,[17] and later modified by Steger and Sorenson,[18] and Middlecoff and Thomas.[19] The present full potential method does not require an orthogonal grid; however, the error introduced by the approximate factorization, Eq. (20), can be minimized if the grid is orthogonal in the cross flow plane (η,ξ). For conical flow calculations, the grid is generated only once, and, as the marching procedure continues, the grid is allowed to grow conically. For a general nonconical body, it would be necessary to construct the grid in every marching plane.

III. Results

Results are presented for both conical and nonconical supersonic flows. Comparisons are made with Euler[3,5] and full potential[9,10] results and experimental data. All the calculations were performed using a CDC 7600 machine.

A. Conical Flows

Besides validating the methodology, computation of conical flows is of interest for generating the initial data plane for nonconical calculations. For a conical geometry (radially invariant), the initial data plane with freestream conditions is chosen at some location $\zeta=\zeta_0$ (usually set at $\zeta=1$). The solution is then marched along ζ using Eq. (20) and boundary conditions. The conical flow calculation is assumed to have converged when the change in the root mean square density is less than 10^{-4}.

Supersonic Leading-Edge Delta Wing

Figure 3 shows the compression surface pressures for a supersonic leading-edge delta wing at $M_\infty=6$, angle of attack $\alpha=-8$ deg, and leading-edge sweep $\Lambda=70$ deg. The present full potential solution compares well with the Euler solution[19] and experimental data. Also shown are the results from the first- and second-order linear theory.[7] Using a 30×40 grid in the (η,ξ) plane, the present approach required 40 iterations to achieve convergence, and 12-15 s of computer time to produce the results shown in Fig. 3.

It is interesting to note that in spite of the limitations of the full potential theory, even at a very high Mach number of 6, the comparison is in reasonable agreement with the Euler

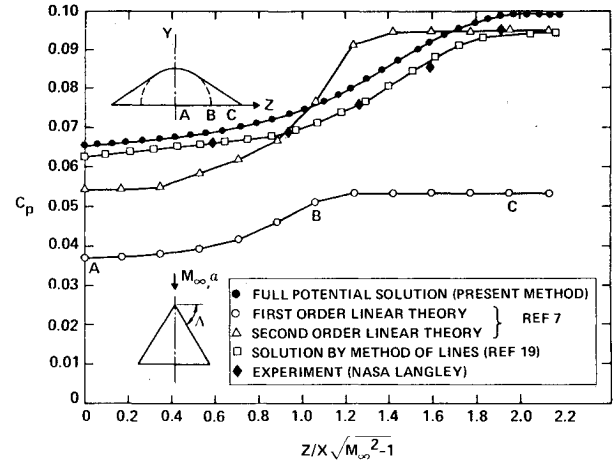

Fig. 3 Predicted compression surface pressure for a 70-deg sweep delta wing at $M_\infty=6$, $\alpha=-8$ deg.

solution and is significantly better than the second-order theory. The discrepancy between the full potential and Euler results is mainly due to neglect of entropy generation in the present approach.

Circular Cone and Ellipse

Figure 4 shows the surface pressure distribution for a circular cone, half angle 7.5 deg, $M_\infty = 3$ at 15 deg angle of attack. At this angle of attack the cross flow Mach number becomes supersonic as the flow turns around the cone from the windward symmetry to the leeward symmetry. This cross flow supersonic region is terminated by the formation of an embedded shock on the cone surface. This is evident from the results of Fig. 4. Grid clustering near the cross flow shock was used both in the Euler calculation of Kutler,[3] and in the present method, to finely resolve the pressure jump. The present calculation required 25 s of computer time, using a 30×60 grid in the (η, ξ) plane.

The liftoff of the vortical singularity on the leeward symmetry plane associated with the formation of the embedded shock is shown in Fig. 5. The location where the contravariant velocity V goes through zero on the leeward symmetry plane ($W = 0$) denotes the location of the vortical singularity. The behavior of the cross flow streamlines converging to the vortical singularity is also shown in Fig. 5.

Figure 6 shows the full potential and Euler cross flow Mach number contours for the circular cone case. The presence of the embedded shock wave in both the results is very clear. The location of the vortical singularity liftoff is also shown in the figure. The Euler result is very oscillatory near the vortical singularity location while the present method predicts a smoother flowfield in the vicinity of the vortical singularity.

The surface pressure distribution on an elliptic cone $\theta_c = 18.39$ deg, $\delta_c = 3.17$ deg at $M_\infty = 1.97$ and $\alpha = 10$ deg is shown in Fig. 7. The results of the present study are compared with Euler calculations of Siclari,[5] full potential results of Grossman,[9] and the linearized thin wing solution of Jones and Cohen.[20] The agreement between the various nonlinear methods is very good, including the position and strength of the embedded shock wave.

Wing-Body Combination

Figure 8 shows the numerically generated grid distribution in the cross flow plane (η, ξ) of a conical wing-body combination. The design of this conically cambered delta wing to achieve shockless recompression is reported in Ref. 21. Figure 9 shows the pressure distribution around this wing-body combination at $M_\infty = 2$, and $\alpha = 7.81$ deg. The leading-edge sweep Λ is 57 deg. The comparison of the results from the present method with the experimental data[21] is excellent. The calculation used a 15×49 grid in the (η, ξ) plane and required less than a minute of computer time.

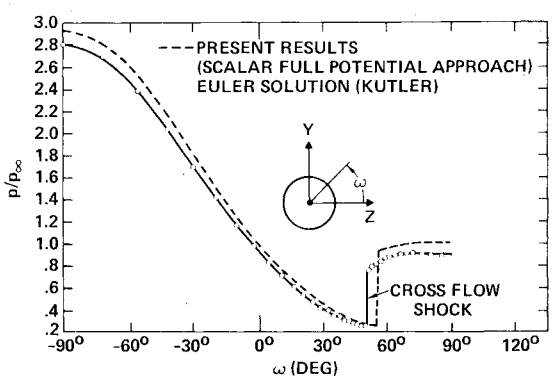

Fig. 4 Surface-pressure distribution for cone at angle of attack; $M_\infty = 3$, $\alpha = 15$ deg, $\theta_c = 7.5$ deg.

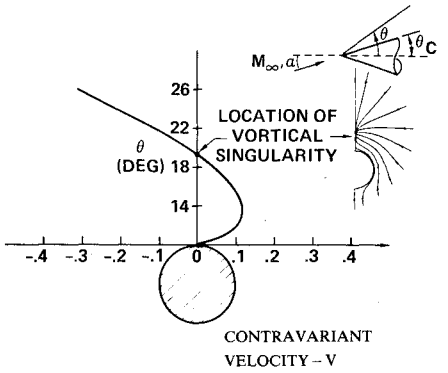

Fig. 5 Vortical singularity liftoff for a circular cone at $M_\infty = 3$, $\alpha = 15$ deg, $\theta_c = 7.5$ deg.

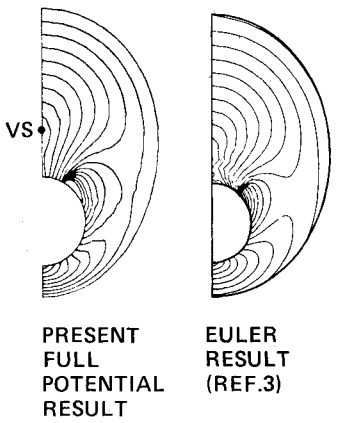

Fig. 6 Comparison of cross flow Mach number contours for cone at angle of attack; $M_\infty = 3$, $\alpha = 15$ deg, $\theta_c = 7.5$ deg (VS = vortical singularity).

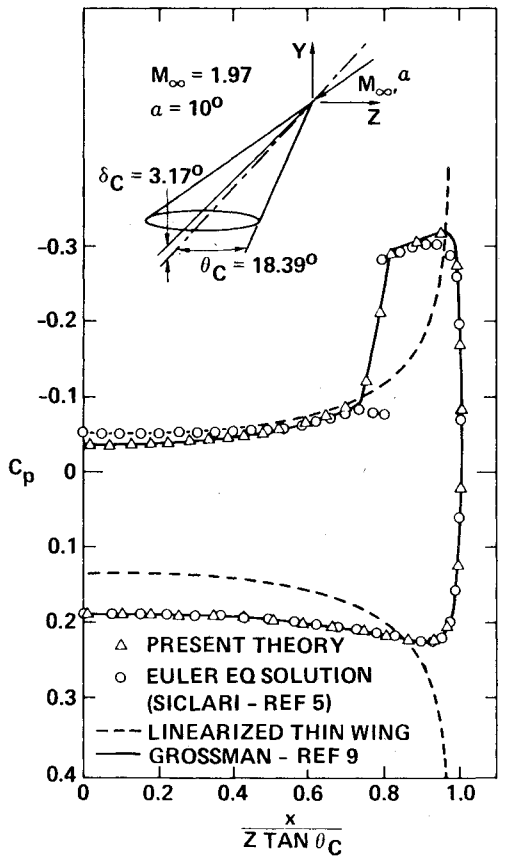

Fig. 7 Surface-pressure distribution on an elliptic cone; $M_\infty = 1.97$, $\theta_c = 18.39$ deg, $\delta_c = 3.17$ deg, $\alpha = 10$ deg.

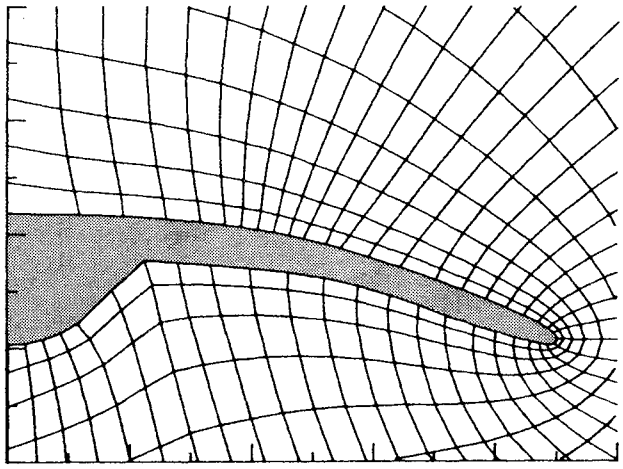

Fig. 8 Computational grid around a wing-body combination.

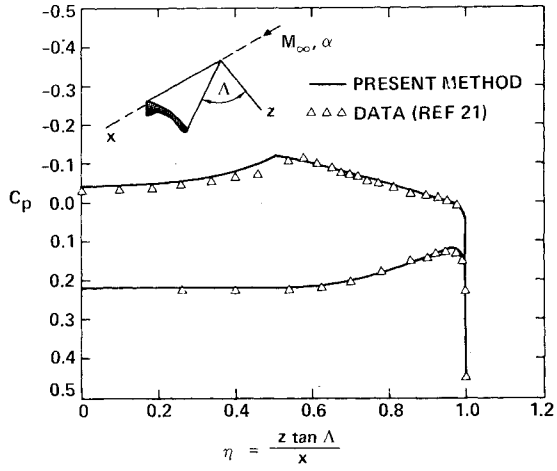

Fig. 9 Surface-pressure distribution for a conically cambered wing-body combination; $M_\infty = 2$, $\alpha = 7.81$ deg, $\Lambda = 57$ deg.

B. Nonconical Flows

Results are also presented for nonconical bodies of revolution and compared with experimental data. The initial data plane for the nonconical marching calculation is first obtained by performing a conical calculation over an assumed very small conical nose. This conical calculation usually takes 20-30 iterations on a typical 30×30 grid in the (η, ξ) plane. The nonconical calculations did not exhibit any increase in computational time over the conical procedure. As mentioned earlier, for the applications considered here where the cross flow station does not vary substantially from the previous one, it was found that there was no need to iterate the solution at each cross flow plane (η, ξ) to converge the density, and plottable accuracy was achieved by simply marching right along the body. However, if the body changes shape appreciably, the current implicit procedure might take 3-5 iterations per cross flow plane to refine the solution.

Reference 22 contains experimental data for several bodies of revolution at various Mach numbers and angles of attack. The shape chosen for comparison here is a circular arc-cylinder body. After the initial data plane was computed using a conical nose assumption, the current method typically used 60 marching steps to reach the end of the body but the calculations are not subject to any step size restriction. A typical calculation required 40-45 s of computer time. Figure 10 shows the circumferential surface pressure distribution at two different axial stations ($x/\ell = 0.225$ and 0.425) for 4 and 8 deg angles of attack at $M_\infty = 2.3$. The results from the present method are compared with experimental data,[22] showing very good agreement for the windward region with some

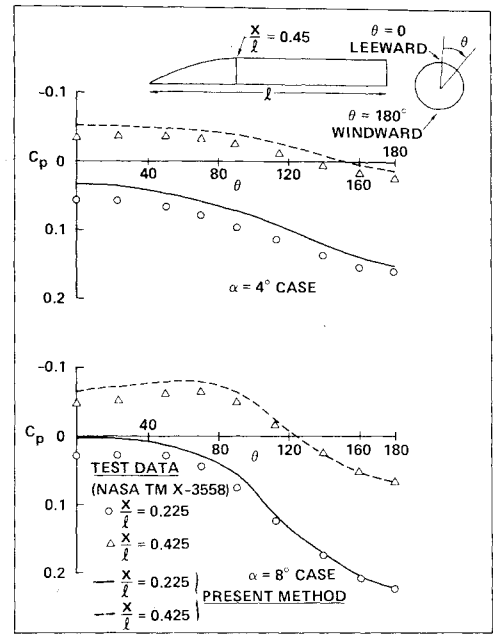

Fig. 10 Circumferential pressure distribution for a circular-arc-cylinder body at $M_\infty = 2.3$.

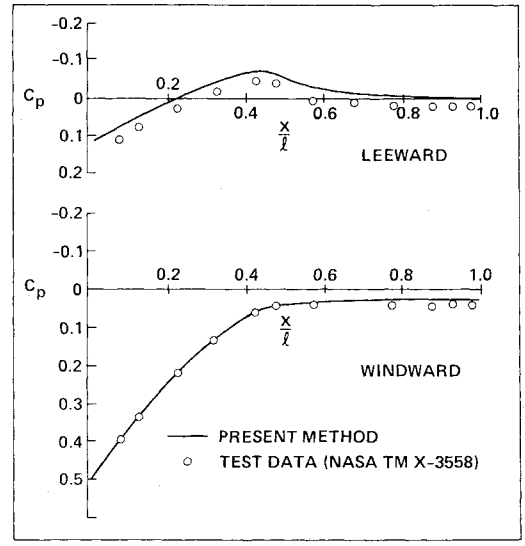

Fig. 11 Surface-pressure distribution for a circular-arc-cylinder body at $\alpha = 8$ deg, $M_\infty = 2.3$.

discrepancy on the leeward side, possibly due to boundary-layer buildup.

Figure 11 shows the surface pressure distribution in the axial direction along the windward and leeward plane of symmetry, at $M_\infty = 2.3$ and $\alpha = 8$ deg. Again, results from the present method compare very well with the experimental data.[22]

IV. Conclusions

An aerodynamic prediction technique based on the full potential equation in conservation form is developed for the treatment of supersonic flowfields. A local density linearization concept and a second-order accurate density biasing scheme are introduced in developing an implicit marching procedure. The method produces results that compare well with Euler solvers, and requires an order of magnitude less computer time and significantly less computer memory over existing Euler codes for the cases presented in the paper. In a subsequent paper,[13] results for more complicated nonconical wing-body flows are presented, along

with a formal theory for the characteristic signal propagation in the cross flow plane.

Acknowledgment

This work was supported in full by NASA Langley Research Center under Contract NAS1-15820.

References

[1] Brooke, D. and Vondrasek, D. V., "Feasibility of Combining Linear Theory and Impact Theory Methods for the Analysis and Design of High Speed Configurations," NASA CR 3069, Dec. 1978.

[2] Woodward, F. A., Tinoco, E. N., and Larsen, J. W., "Analysis and Design of Supersonic Wing-Body Combinations, Including Flow Properties in the Near Field. Part I—Theory and Application," NASA CR 73106, 1967.

[3] Kutler, P., "Computation of Three-Dimensional, Inviscid Supersonic Flows," *Lecture Notes in Physics*, Vol. 41, Springer-Verlag, New York, 1975, pp. 293-374.

[4] Marconi, F., Salas, M., and Yeager, L., "Development of a Computer Code for Calculating the Steady Super/Hypersonic Inviscid Flow Around Real Configurations, Vol. I—Computational Techniques," NASA CR 2675, April 1976.

[5] Siclari, M. J., "Investigation of Cross Flow Shocks on Delta Wings in Supersonic Flow," *AIAA Journal*, Vol. 18, Jan. 1980, p. 85.

[6] Moretti, G., "Conformal Mappings for the Computation of Steady Three-Dimensional Supersonic Flows," *Numerical/Laboratory Computer Methods in Fluids Mechanics*, edited by A. A. Pouring and V. I. Shah, ASME, New York, 1979, pp. 13-28.

[7] "Formulation of Aerodynamic Prediction Techniques for Hypersonic Configuration Design," NASA CR 158994, Feb. 1979.

[8] Gunness, R. C. Jr., Knight, C. J., and Sylvia, E. D., "Flow Field Analysis of Aircraft Configurations using a Numerical Solution to the Three-Dimensional Unified Supersonic/Hypersonic Small-Disturbance Equations," NASA CR 1926, Feb. 1972.

[9] Grossman, B., "Numerical Procedure for the Computation of Irrotational Conical Flows," *AIAA Journal*, Vol. 17, Aug. 1979, pp. 828-837.

[10] Grossman, B. and Siclari, M. J., "The Nonlinear Supersonic Potential Flow over Delta Wings," AIAA Paper 80-0269, Jan. 1980.

[11] Jameson, A., "Transonic Potential Flow Calculations using Conservation Form," *AIAA Second Computational Fluid Dynamics Conference Proceedings*, 1975, pp. 148-155.

[12] Lax, P. D., "Weak Solutions of Nonlinear Hyperbolic Equations and Their Numerical Computation," *Communications on Pure and Applied Mathematics*, Vol. 7, No. 1, 1954, pp. 159-193.

[13] Shankar, V. and Osher, S., "An Efficient Full Potential Implicit Method Based on Characteristics for Analysis of Supersonic Flow," AIAA Paper 82-0974, June 1982.

[14] Jameson, A. and Caughey, D. A., "A Finite Volume Method for Transonic Potential Flow Calculations," AIAA Paper 77-635, June 1977.

[15] Holst, T. L., "A Fast, Conservative Algorithm for Solving the Transonic-Potential Equation," AIAA Paper 79-1456, July 1979.

[16] Steger, J. L. and Caradona, F. X., "A Conservative Implicit Finite Difference Algorithm for the Unsteady Transonic Full Potential Equation," Flow Simulations, Inc. Rept. 79-04, Dec. 1979.

[17] Thompson, J. F., Thames, F. C., and Mastin, C. W., "TOMCAT—A Code for Numerical Generation of Boundary-Fitted Curvilinear Coordinate Systems on Fields Containing Any Number of Arbitrary Two-Dimensional Bodies," *Journal of Computational Physics*, Vol. 24, 1977, p. 274.

[18] Steger, J. L. and Sorenson, R. L., "Automatic Mesh-Point Clustering Near a Boundary in Grid Generation with Elliptic Partial Differential Equations," *Journal of Computational Physics*, Vol. 33, Dec. 1979, p. 405.

[19] South, J. C. and Klunker, E. B., "Method for Calculating Nonlinear Conical Flows," NASA SP-228, 1969, pp. 131-158.

[20] Jones, R. T. and Cohen, D., *High Speed Wing Theory*, Princeton University Press, Princeton, N.J., 1960, pp. 157, 160.

[21] Miller, D. S., Landrum, E. J., Townsend, J. C., and Mason, W. H., "Pressure and Force Data for a Flat Wing and a Warped Conical Wing Having a Shockless Recompression at Mach 1.62," NASA TP 1759, April 1981.

[22] Landrum, E. J., "Wind Tunnel Pressure Data at Mach Numbers from 1.6 to 4.63 for a Series of Bodies of Revolution at Angles of Attack from −4 to 60°," NASA TM X-3558, Oct. 1977.